Biomedical Optics EXPRESS

Optically monitored drug delivery patch based on porous silicon and polymer microneedles

Principia Dardano,[1] Alessandro Caliò,[1,2] Jane Politi,[1,3] Ilaria Rea,[1] Ivo Rendina,[1] and Luca De Stefano[1,*]

[1]*National Research Council - Institute for Microelectronics and Microsystems, Via P. Castellino 111, 80131, Naples, Italy*
[2]*University of Naples Federico II - Department of Physical Science, Via Cinthia, 80100, Naples, Italy*
[3]*University of Naples Federico II - Department of Chemical Science, Via Cinthia, 80100, Naples, Italy*
[*]*luca.destefano@cnr.it*

Abstract: Fabrication and characterization of an optically monitored hybrid patch for local administration of drugs, based on polymeric micro-needles and a porous silicon free-standing membrane, are reported. The micro-needles are realized by an innovative photolithographic approach that allows fine tuning of geometrical parameters, using polyethylene glycol and a commercial photo-catalyzer. The porous silicon multilayer not only increases the storage of a relevant amount of the drug, but also offers a continuous, naked-eye monitoring of the drug delivery process. As a proof-of-concept experiment, we report our results on the release of a dye molecule (fluorescein, 332 Da) in a phosphate saline buffer.

OCIS codes: (170.0170) Medical optics and biotechnology; (310.6845) Thin film devices and applications; (160.5470) Polymers

References and links

1. S. Henry, D. V. McAllister, M. G. Allen, and M. R. Prausnitz, "Microfabricated Microneedles: A Novel Approach to Transdermal Drug Delivery," J. Pharm. Sci. **87**(8), 922–925 (1998).
2. E. V. Mukerjee, S. D. Collins, R. R. Isseroff, and R. L. Smith, "Microneedle array for transdermal biological fluid extraction and in situ analysis," Sens. Actuators A Phys. **114**(2-3), 267–275 (2004).
3. P. R. Miller, S. A. Skoog, T. L. Edwards, D. M. Lopez, D. R. Wheeler, D. C. Arango, X. Xiao, S. M. Brozik, J. Wang, R. Polsky, and R. J. Narayan, "Multiplexed Microneedle-based Biosensor Array for Characterization of Metabolic Acidosis," Talanta **88**, 739–742 (2012).
4. M. R. Prausnitz and R. Langer, "Transdermal drug delivery," Nat. Biotechnol. **26**(11), 1261–1268 (2008).
5. S. Kaushik, A. H. Hord, D. D. Denson, D. V. McAllister, S. Smitra, M. G. Allen, and M. R. Prausnitz, "Lack of Pain Associated with Microfabricated Microneedles," Anesth. Analg. **92**(2), 502–504 (2001).
6. M. R. Prausnitz, "Reversible skin permeabilization for transdermal delivery of macromolecules," Crit. Rev. Ther. Drug Carrier Syst. **14**(4), 455–483 (1997).
7. E. M. Cahill and E. D. O'Cearbhaill, "Toward Biofunctional Microneedles for Stimulus Responsive Drug Delivery," Bioconjug. Chem. **26**(7), 1289–1296 (2015).
8. L. Ventrelli, L. Marsilio Strambini, and G. Barillaro, "Microneedles for Transdermal Biosensing: Current Picture and Future Direction," Adv. Healthc. Mater. **4**(17), 2606–2640 (2015).
9. N. Wilke, A. Mulcahy, S.-R. Ye, and A. Morrissey, "Process optimization and characterization of silicon microneedles fabricated by wet etch technology," Microelectronics J. **36**(7), 650–656 (2005).
10. F. Chabri, K. Bouris, T. Jones, D. Barrow, A. Hann, C. Allender, K. Brain, and J. Birchall, "Microfabricated silicon microneedles for nonviral cutaneous gene delivery," Br. J. Dermatol. **150**(5), 869–877 (2004).
11. M. B. Mellott, K. Searcy, and M. V. Pishko, "Release of protein from highly cross-linked hydrogels of poly(ethylene glycol) diacrylate fabricated by UV polymerization," Biomaterials **22**(9), 929–941 (2001).
12. G. Valdés-Ramírez, J. R. Windmiller, J. C. Claussen, A. G. Martinez, F. Kuralay, M. Zhou, N. Zhou, R. Polsky, P. R. Miller, R. Narayan, and J. Wang, "Multiplexed and switchable release of distinct fluids from microneedle platforms via conducting polymer nanoactuators for potential drug delivery," Sens. Actuators B Chem. **161**(1), 1018–1024 (2012).
13. M. W. Ashraf, S. Tayyaba, and N. Afzulpurkar, "Micro Electromechanical Systems (MEMS) Based Microfluidic Devices for Biomedical Applications," Int. J. Mol. Sci. **12**(6), 3648–3704 (2011).
14. J. L. Tan, J. Tien, D. M. Pirone, D. S. Gray, K. Bhadriraju, and C. S. Chen, "Cells lying on a bed of microneedles: An approach to isolate mechanical force," Proc. Natl. Acad. Sci. U.S.A. **100**(4), 1484–1489 (2003).

#253445 Received 6 Nov 2015; revised 9 Feb 2016; accepted 22 Feb 2016; published 4 Apr 2016

15. R. Vecchione, S. Coppola, E. Esposito, C. Casale, V. Vespini, S. Grilli, P. Ferraro, and P. A. Netti, "Electro-Drawn Drug-Loaded Biodegradable Polymer Microneedles as a Viable Route to Hypodermic Injection," Adv. Funct. Mater. **24**(23), 3515–3523 (2014).
16. R. F. Donnelly, T. R. R. Singh, M. J. Garland, K. Migalska, R. Majithiya, C. M. McCrudden, P. L. Kole, T. M. T. Mahmood, H. O. McCarthy, and A. D. Woolfson, "Hydrogel-forming microneedle arrays for enhanced transdermal drug delivery," Adv. Funct. Mater. **22**(23), 4879–4890 (2012).
17. J. R. Henstock, L. T. Canham, and S. I. Anderson, "Silicon: The evolution of its use in biomaterials," Acta Biomater. **11**, 17–26 (2015).
18. L. De Stefano, L. Moretti, I. Rendina, and A. M. Rossi, "Time-resolved sensing of chemical species in porous silicon optical microcavity," Sens. Actuators B Chem. **100**(1-2), 168–172 (2004).
19. I. Rendina, I. Rea, L. Rotiroti, and L. De Stefano, "Porous Silicon Based Optical Biosensors and Biochips," Physica E **38**(1-2), 188–192 (2007).
20. L. De Stefano, M. Rossi, M. Staiano, G. Mamone, A. Parracino, L. Rotiroti, I. Rendina, M. Rossi, and S. D'Auria, "Glutamine-binding protein from Escherichia coli specifically binds a wheat gliadin peptide allowing the design of a new porous silicon-based optical biosensor," J. Proteome Res. **5**(5), 1241–1245 (2006).
21. L. De Stefano, I. Rea, P. Giardina, A. Armenante, and I. Rendina, "Protein modified porous silicon nanostructures," Adv. Mater. **20**(8), 1529–1533 (2008).
22. P. Dardano, A. Caliò, V. Di Palma, M. F. Bevilacqua, A. Di Matteo, and L. De Stefano, "Photolithographic approaches to polymeric microneedles array fabrication for biomedical applications," Materials (Basel) **8**(12), 8661–8673 (2015).
23. R. F. Donnelly, T. R. Raj Singh, and A. D. Woolfson, "Microneedle-based drug delivery systems: Microfabrication, drug delivery, and safety," Drug Deliv. **17**(4), 187–207 (2010).
24. E. Larrañeta, J. Moore, E. M. Vicente-Pérez, P. González-Vázquez, R. Lutton, A. D. Woolfson, and R. F. Donnelly, "A proposed model membrane and test method for microneedle insertion studies," Int. J. Pharm. **472**(1-2), 65–73 (2014).
25. H. Li, Y. Yu, S. Faraji Dana, B. Li, C.-Y. Lee, and L. Kang, "Novel engineered systems for oral, mucosal and transdermal drug delivery," J. Drug Target. **21**(7), 611–629 (2013).
26. Prof. L. T. Canham, pSiMedica Ltd, Malvern Hills Science Park, Malvern, Worcerstershire, WR14 35Z, UK, private communication.
27. J. S. Kochhar, W. X. S. Lim, S. Zou, W. Y. Foo, J. Pan, and L. Kang, "Microneedle Integrated Transdermal Patch for Fast Onset and Sustained Delivery of Lidocaine," Mol. Pharm. **10**(11), 4272–4280 (2013).

1. Introduction

Microneedles (MNs) are actually flexible devices, which enable innovative and breakthrough applications in biomedicine, both in diagnostics and therapeutics [1–3]. The development of MNs has been driven in the first by finding a painless alternative to hypodermic injections, and interesting devices based on MNs are currently progressing through clinical trials for delivery of molecules and vaccines, such as insulin, parathyroid hormone and influenza vaccine [4]. More extended functions have been imagined since it became clear that MNs were the almost perfect interface between the derma and any medical device for theranostic [5]. As a matter of fact, MNs permit exchanges between outside of the human body and the interstitial liquid under the stratum corneum, which is the first layer of the skin practically impermeable to all molecules with molecular weight (MW) larger than 500 Dalton [6]. This is the main limit to transdermal drug delivery: in order to be a really alternative approach to oral or systemic (i.e. intravenous) administration, also biomolecules like protein or antibodies (MW >kDa or even hundreds of kDa) should be carried in the organism. Once the barrier of epithelial tissue is broken by the tip of a MN, it is possible to use this channel for enhanced monitoring of substances with minimum risk and invasiveness. Continuous monitoring of glucose, lactate, and pH has been demonstrated [7]. Well-established micro- and nano-fabrication techniques allow low-cost production of MNs by hard constituents, such as crystalline silicon and related materials (i.e. porous silicon, silicon dioxide and nitride, and so on) [8], ceramics and metals [9, 10] as well as by soft ones, mainly polymers and hydrogels [11, 12]. As usual, each material choice has its own pros and cons: for example, silicon can be structured with nanometric precision and quite directly integrated with electronics and actuators in the same device, but, on the other hand, due to its fragility, it could cause local irritation and infection. Polymeric materials have been proved to be promising for their biocompatibility and versatility, even if there are some production restrictions (large scale integration is not still possible) that should be overcome. Since their appearance on the

#253445 Received 6 Nov 2015; revised 9 Feb 2016; accepted 22 Feb 2016; published 4 Apr 2016

biomedical scene, a lot of efforts have been made to fabricate biocompatible tailored MNs: shape, length and other mechanical properties can be properly customized to the specific application [13–16].

In this paper, we present a hybrid structure based on porous silicon (PSi) and polymeric MNs that is proposed as a proof-of-concept device for transdermal drug delivery. PSi is a porous material largely used in drug administration, from oral formulation to cellular uptake: its sponge-like morphology can be usefully used for load drugs and any kind of molecules, since its surface can be chemically modified [17]. Moreover, PSi structures can be optically encoded, which means that they can exhibit specific photonic signatures [18]. The fabrication of MNs has been realized by photolithography of a PolyEthylene Glycol DiAcrylate (PEGDA) hydrogel mixture with a commercial photo-catalyzer. The device includes a PSi free-standing membrane with a Bragg mirror optical structure (PSiBM) which reflects a specific bright color in the visible. Furthermore, the PSiBM has a double function: it acts as a drug/molecules reservoir, and, since its color changes depending on what fills its pores, it can be used to optically monitor the drug released by diffusion in the MNs, and from MNs to the skin.

2. Materials and methods

All chemicals were reagent grade or higher, and were used as received unless otherwise specified. Crystalline silicon was provided by Silicon Materials. Hydrofluoric acid (HF) 48%, absolute ethanol, fluorescein ($C_{20}H_{12}O_5$, MW 332Da), PolyEthylene (Glycol) DiAcrylate (PEGDA, average molecular weight, MW = 250) and phosphate buffered saline (PBS) were obtained from Sigma Aldrich. 2-Hydroxy-2-methyl-1-phenyl-propan-1-one (Darocur 1173) was provided by BASF. PEGDA is a biologically inert hydrogel that gels rapidly at room temperature in presence of photo-initiator and UV light, so that it is possible to fabricate PEGDA microneedles by means of a direct exposition to UV light. Darocur is a liquid photo-initiator which is used to start the photo-polymerization of chemically unsaturated pre-polymer solution. Fluorescein is a synthetic organic compound, whose molecular weight is 332 Da, and it was used as fluorescent dye in drug loading and release.

2.1. Fabrication process

2.1.1. Free-standing porous silicon Bragg mirror

Photonic structures based on free-standing porous silicon membranes were fabricated by electrochemical etching of p^{++} crystalline silicon (0.001 Ωcm resistivity, <100> oriented, 500 μm thick) in hydrofluoric acid (HF, 50% in volume), water, and ethanol solution (1:1:1), in dark and at room temperature. Before anodization dissolution, silicon substrate was immersed in HF solution for two minutes in order to remove native oxide layer. Time breaks of 5 s were used during etching process in order to recover HF concentration at dissolution edge and start next layer formation with zero current density: in this way, density current is always the same for each layer. For all structures, the etching area is 0.98 cm^2. From the optical point of view, the porous silicon membrane behaves as a Bragg mirror. It is a periodic structure with alternating layers of low (n_L) and high (n_H) refractive index, or high (P_H) and low (P_L) porosity, respectively, whose thicknesses satisfy the relation $2(n_H d_H + n_L d_L) = m\lambda_B$, where m is the order of the Bragg condition [19]. The layer stack is usually denoted as $[n_L n_H]N$, where N is the number of periods. In this work, the Bragg mirror was made by 30 periods. High porosity (72.6%) layers were obtained applying a current density of 200 mA/cm^2 (anodization potential average value 1.9 ± 0.3 V) for 0.6 s (n_L = 1.6, d_L = 78 nm); low porosity (68.4%) layers were obtained applying a current density of 100 mA/cm^2 (anodization potential average value 1.1 ± 0.4 V) for 0.87 s (n_H = 1.75, d_H = 65. nm). Porosities and thicknesses have been estimated by spectroscopic ellipsometry measurements (data not shown here) on each sample. Values of refractive index were calculated at λ = 500 nm by using a Bruggeman

#253445 Received 6 Nov 2015; revised 9 Feb 2016; accepted 22 Feb 2016; published 4 Apr 2016

approximation [20, 21]. At the end of the porous multilayer formation, the anodization current density was quickly increased up to 600 mA/cm^2 (anodization potential average value 16.2 ± 0.9 V) for 3 s and then to 800 mA/cm^2 (anodization potential average value 25.1 ± 1.0 V) for 5 s, in order to turn the reaction into the electrochemical polishing state and separate the porous silicon membrane from the silicon substrate. The floating porous silicon membrane was thick about 4.29µm and has been oxidized into absolute ethanol solution for 24 hours at room temperature.

2.1.2. Microneedles array fabrication

A self-standing microneedles array has been fabricated by means of the photolithography technique, using as photoresist a solution of PEGDA and Darocur at 2% volume/volume concentration. This solution behaves as a negative photoresist, i.e. on exposure to UV light the photoresist crosslinks and it is less soluble in the developer solution then the unexposed areas. The flow chart of the fabrication of the microneedles is showed in Fig. 1.

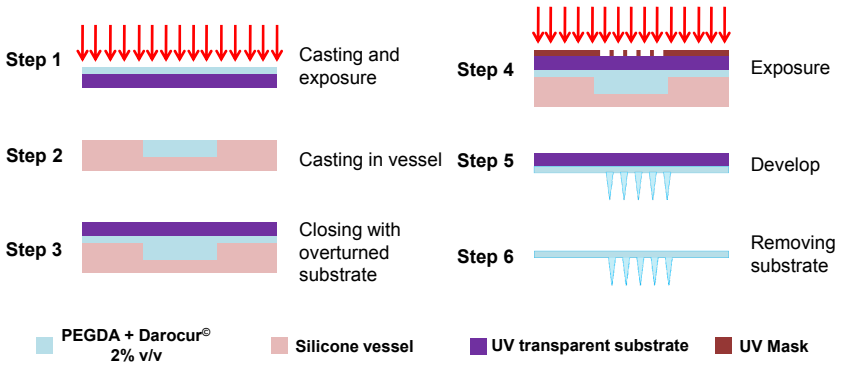

Fig. 1. Microneedles array process flow: photolithographic standard approach allows low cost fabrication of large area MNs array. Steps 1-6 are recalled in text in Fabrication process paragraph.

1 ml of PEGDA based photoresist solution was deposited on a quartz substrate by drop casting and then it was hardened by exposure to UV light for 10 s, obtaining about 1 mm thick layer (Fig. 1, step 1). A silicone vessel (1.6x2.0x0.44 cm) was filled with the PEGDA solution (1.41 mL) (Fig. 1, step 2) and closed by the hardened PEGDA on quartz (Fig. 1, step 3). In this way, the PEGDA solution and the hardened PEGDA were in direct contact and the bases of microneedles have been attached to the PEGDA layer on the quartz. Exposure time to UV light was 7.5 s at 18 mW/cm^2 with a quartz/chrome photomask in soft contact to the quartz layer (Fig. 1, step 4). Finally, the sample was developed in deionized water for 2 minutes (Fig. 1, step 5), in order to remove the unpolymerized photoresist, and dried in nitrogen. The quartz was separated from the layer of photoresist by means of a cutter, obtaining a free-standing microneedles array (Fig. 1, step 6). More details on MNs array fabrication can be found on our recent publication [22].

2.1.3. Patch assembling

The final device was fabricated by assembling the porous silicon membrane and the microneedles array as showed in Fig. 2.

#253445 Received 6 Nov 2015; revised 9 Feb 2016; accepted 22 Feb 2016; published 4 Apr 2016

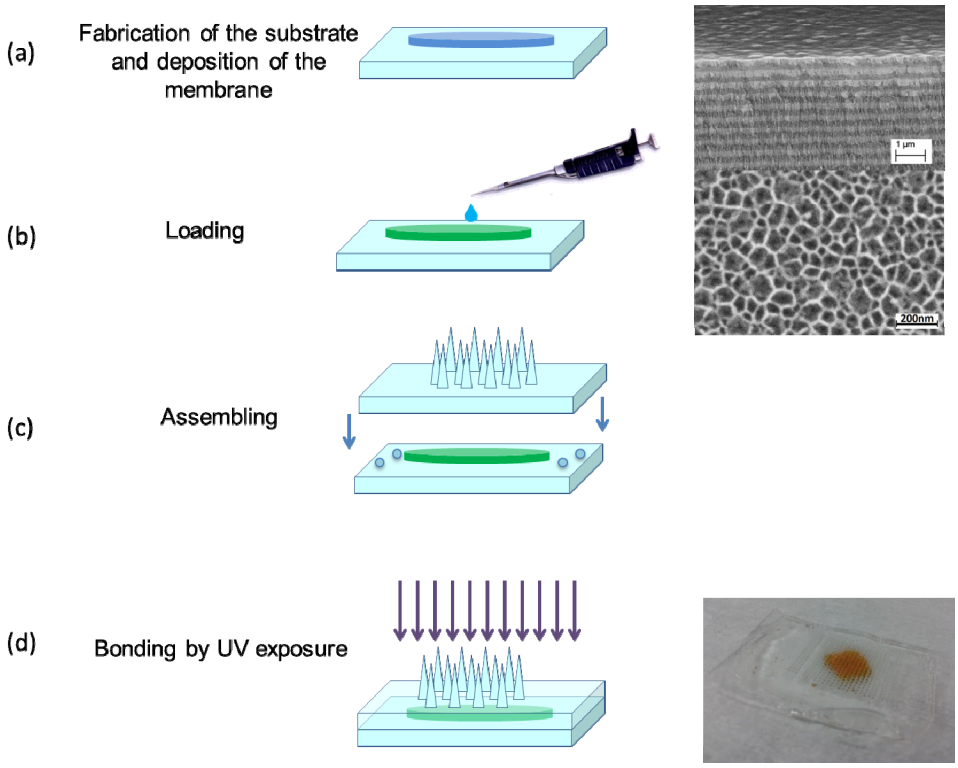

Fig. 2. Schematic of hybrid patch assembling: the porous silicon oxidized free-standing membrane is placed on PEGDA support (a); then the active molecules are loaded in its spongy matrix (b) and the MNs array is bonded by UV exposure (c and d). In the inset, microphotograph by electron scanning microscopy of PSi real sample and a digital image of the assembled patch are reported.

The ethanol with the floating PSi oxidized membrane was casted on the hardened PEGDA-quartz support (Fig. 2(a)) and dried at room temperature. Then, the dry membrane has been loaded by drop casting technique by 50 µl of saturated aqueous solution of fluorescein (Fig. 2(b)). The PSi drug reservoir was blocked and sealed by bonding the microneedles array to the PEGDA-quartz support (Fig. 2(c)): drops of 50 µl of liquid photoresist have been poured around porous silicon membrane in order to create a sandwich-like final device. The exposure to UV (10 s, 18 mW/cm^2) resulted in the final hybrid device, ready to be used (Fig. 2(d)). UV bonding is very fast and in case of specific UV sensitive drugs, this sealing procedure can be replaced by standard glue application. In order to evaluate the release of molecules at hematic pH, the microneedles patch device was immersed in a solution of PBS 1X at pH 7.2 for 2, 4, 8 and 24 hours. Reflectivity spectra, fluorescence intensities and digital images of device has been acquired and compared.

2.2. Characterization techniques

2.2.1. Spectroscopic reflectometry

The reflectivity spectra of porous silicon photonic structures have been acquired using the spectrometer of the thin film analyzer FILMETRICS Model F20: a white light was sent on the sample by means of a Y optical reflection probe. The same probe was used to pick up and guide the light reflected to the sensor. Spectra have been acquired at normal incidence in the wavelength range 380-650 nm, without any optical filter. At least three measurements have been recorded to have an average spectrum of the sample.

#253445 Received 6 Nov 2015; revised 9 Feb 2016; accepted 22 Feb 2016; published 4 Apr 2016

2.2.2. Fluorescence microscopy

Fluorescence analysis was performed by means of Leica Z16 APO fluorescence macroscope equipped with the Leica DFC300 camera. The light source is a mercury-based lamp (ebq100 mc-l by Leistungs elektronik JENA GmbH). Optics used for acquisition was a 450-490 nm band-pass excitation filter, a 510 nm dichromatic mirror, and a 515 nm suppression filter. Fluorescence values reported in the work are averages of three measurements. Images analysis was performed by means of ImageJ, a public domain, Java-based image-processing program.

2.2.3. Digital photography

Images of the device were acquired by a digital camera with a photographic objective (5x), an 8 mega pixel CMOS sensor, and equipped by a white LED flash source. Maximum resolution of photos is 3264 x 2448 pixels.

3. Results and discussion

We recently proposed a photolithographic approach to polymeric MNs production that offered several advantages with respect to other micro-fabrication techniques, such as replica molding, laser sculpturing, surface micromachining or three-dimensional printing [23]. We demonstrated in a systematic study that this technique could allow low-cost fabrication of MNs array with very finely tunable geometric features: shape, length and diameter can be easily changed by properly adjusting the process parameters (lamp power, exposition time, and photolithographic mask) [22]. The results of the photolithographic fabrication process are summarized in Fig. 3: on the left photographs column, the MNs array flexibility (Fig. 3(a)) and a macroscopic view of MNs (Fig. 3(c)) are shown. PEGDA assures a smooth and soft device that can be deformed without breaking. The ensemble of MNs is a hexagonal array of ten rows, each needle having 400 µm base diameter and spaced by 866 µm. On the right column, micro-images of a single needle (Fig. 3(b)) and tip measurement (Fig. 3(d)) are reported: the overall length is about 1420 µm and the MN head has a curvature radius of 11.6 µm. The ability to indent the skin has been estimated by mimicking penetration in Parafilm as reported in the paper of Larrañeta et. al. (data not shown here) [24].

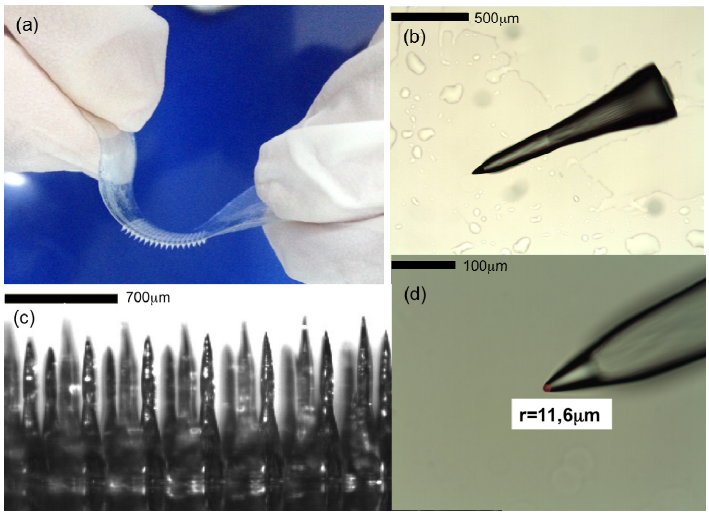

Fig. 3. MNs array characterization: (a) MNs array flexibility; (b) micro-images of a single needle; (c) macroscopic view of MNs; (d) tip measurement. The MNs array on PEGDA has good flexibility useful for patch applications. The MNs have highness, shapes and curvature radii tunable by changing process parameters.

#253445 Received 6 Nov 2015; revised 9 Feb 2016; accepted 22 Feb 2016; published 4 Apr 2016

The hybrid patch included a porous silicon membrane in order to administer and to monitor drug release, simultaneously. A sketch of the device operation is shown in Fig. 4: the PSiBM was firstly loaded by the drug (Fig. 4(a)), then the drug diffused into the PEGDA polymeric matrix of the MNs (Fig. 4(b)) and, finally, the drug was released into the external solution (Fig. 4(c)).

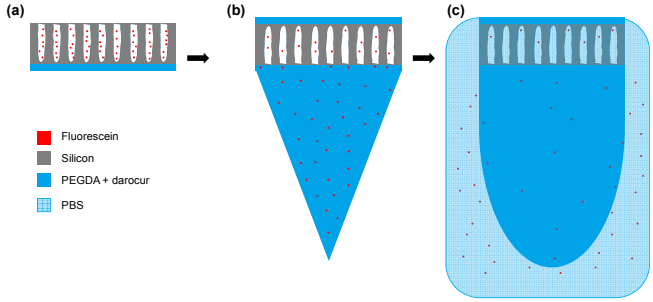

Fig. 4. Sketch of device operation: the PSiM is loaded with fluorescein molecules (a), fluorescein diffuses into the MNs nanoporous (b) and it is released into the PBS solution as effect of the MNs swelling(c).

Since we would like to visualize and properly image the molecule release process, we used, as a proof of concept, a dye molecule, 332 Da fluorescein, and PBS 1X solution at pH 7.2 as mimic of human interstitial liquid.

Fluorescent images reported in Fig. 5 experimentally confirm the diffusion of fluorescein from the PSi reservoir into the PEGDA polymeric matrix of the MNs. The migration of the luminescent molecules from PSi to MNs started just after the bonding of device constituents and spontaneously occurred, also in absence of the external solution.

#253445 Received 6 Nov 2015; revised 9 Feb 2016; accepted 22 Feb 2016; published 4 Apr 2016

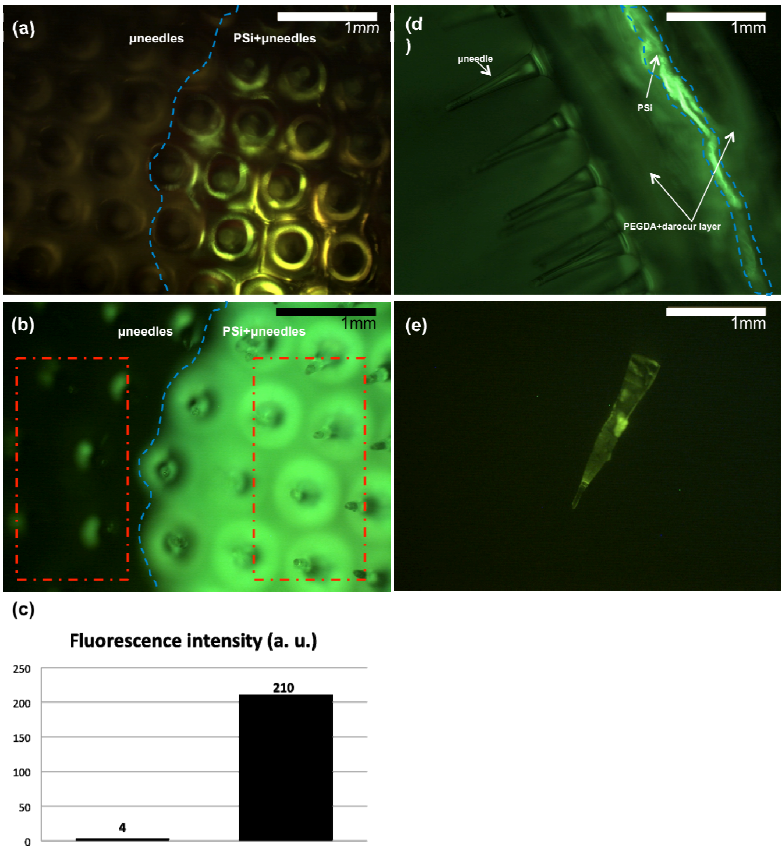

Fig. 5. (a) Top view of the device acquired in bright field mode: the blue line underlines the profile of the porous silicon membrane placed under the microneedles (right side) with respect to the only microneedles (left side); (b) Top view of the device acquired in fluorescence mode with the same field of view of (a): the image shows that only the area overlapping the porous silicon membrane is fluorescent (right side). (c) Fluorescence intensity of areas inside the red rectangles calculated using ImageJ software; (d) Lateral view of the device acquired in fluorescence mode: the blue line underlines the profile of the porous silicon membrane placed under the microneedles. (e) A single microneedle detached from the device after fluorescein loading shows that the fluorescein is almost uniformly distributed from the base to the tip.

A comparison between partial top views of device, one acquired in bright field mode (Fig. 5(a)) and the other in fluorescence mode (Fig. 5(b)), clearly shows the edge of the PSiMB, highlighting that only the area of MNs array overlapping the PSiMB was fluorescent. A quantitative estimation (see data reported in Fig. 5(c)), given by counting the fluorescence intensity of the area inside the red rectangle, revealed a value of 210 counts, in case the PSiMB was just under the MNs array (right side of Fig. 5(b)), and only 4 counts where only MNs were imaged outside the area of the PSiMB (left side of Fig. 5(b)). This was also a proof that polymeric MNs did not show intrinsic fluorescence signal. Cross section of the whole device (Fig. 5(d)) and picture of a single MN, detached from the PEGDA support (Fig. 5(e)), have been acquired in fluorescence mode. Both images shown that the fluorescein was almost uniformly distributed from the base to the tip of the MNs: this result proved that the fluorescein molecules were not chemically bonded neither mechanically fixed into the polymeric matrix and could easily diffuse from the PSiMB mesoporous layer to the nanoporous polymeric matrix [25]. The diffusion naturally stopped when equilibrium between the fluorescein concentration into the PSiMB and the rest of the device was reached. Time constant of diffusion was estimated by microgravimetry (data not shown here) as about 2

#253445 Received 6 Nov 2015; revised 9 Feb 2016; accepted 22 Feb 2016; published 4 Apr 2016

minutes. The PSiMB was not only a physical tank for drug load, but also a naked-eye optical monitor of what was happening to the molecules stored in the porous layer: the color of the PSiMB, due to the photonic stop band in the visible region of the wavelength spectrum, changed as a function of the porous layer drug content.

In Fig. 6(a), the reflectivity spectra of the PSiMB after oxidation, fluorescein loading and PBS immersion after 2 hours are shown.

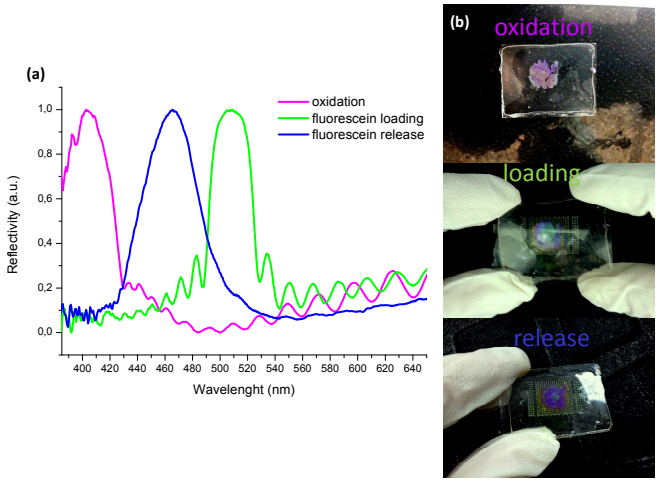

Fig. 6. Spectroscopic reflectometry (a) and naked eye (b) characterizations after oxidation, fluorescein loading and release.

The Bragg multilayer, i.e. a stack of alternating films with proper thicknesses and refractive indexes which satisfy the Bragg relationship, is an interferometric mirror that exhibits maximum reflection for a specific interval of wavelengths, the so called stop band, in our case between 432 and 464 nm. The stop band shifts if thicknesses or refractive indexes are modified: is this the case of porous silicon based Bragg mirror where the stop band position depends on the porosity of the stack. When the PSiMB was filled by molecules, the optical spectrum red shifted towards higher wavelengths, since the material appeared denser on average: in case of fluorescein loading more than 100 nm of red-shift was measured (Fig. 6(a), green curve). By water contact angle measuring the volume of solution penetrated in the sponge-like structure (data not shown here), we estimated up to 37,5 μg of fluoresceine loaded in the device.The new position of the resonant wavelength was stable after bonding and sealing: the diffusion of fluorescein in the PEGDA matrix did not strongly modify the optical spectrum, i.e. there was not a relevant depletion of the PSi reservoir. Moreover the red-shift was proportional to fluorescein concentration in solution, as demonstrated by measurements reported in Fig. 7: the optical spectra in presence of solvent and different concentration of fluorescein were registered without any optical filter and they are reported in Fig. 7(a) together with the calibration curve (Fig. 7(b)). The calibration curve showed the relation between the optical response of the Bragg mirror and the fluorescein concentration loaded. Curve highlighted that higher the fluorescein stored in the porous silicon structure, the higher is the red shift of the reflectivity spectrum of the optical structure. On the contrary, a strong blue shift (more than 50 nm) of the spectra, observed after immersion in PBS, proved the release of fluorescein from the PSiMB. The shifts of the optical spectrum corresponded to changes in color of the device, which can be clearly monitored by naked eye, as shown in Fig. 6(b). In Table 1, the spectroscopic reflectometry data relative to the absolute position of the wavelength peak and the blue shift of Bragg optical structure peak are reported as function of immersion time in PBS.

#253445 Received 6 Nov 2015; revised 9 Feb 2016; accepted 22 Feb 2016; published 4 Apr 2016

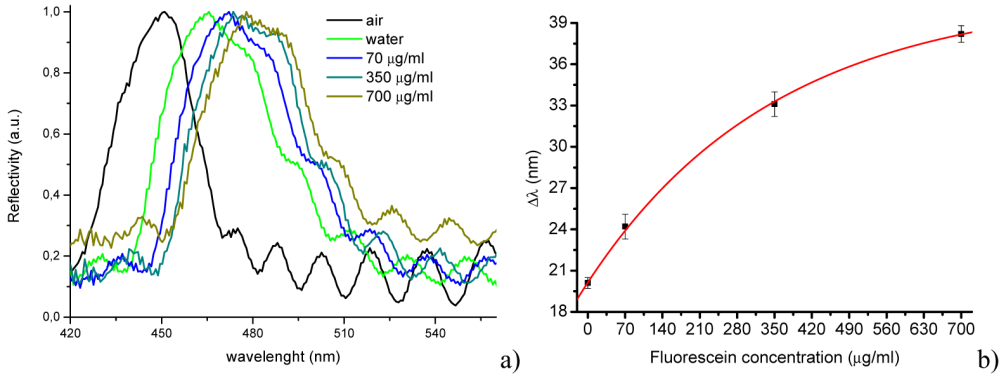

Fig. 7. Calibration curve of fluorescein loading into Bragg mirror optical structure b); correspondent optical spectra a).

Table 1. Spectroscopic reflectometry data of absolute position and shift of Bragg optical structure peak as function of immersion time in phosphate buffer saline.

	Before PBS	After 2h PBS	After 4h PBS	After 8h PBS	After 24h PBS
Peak position	508.2 ± 0.3	450.5 ± 0.4	444.9 ± 0.5	445.6 ± 0.9	436.6 ± 0.2
Blue shift	-	57.7 ± 0.1	63.3 ± 0.1	62.7 ± 0.2	71.6 ± 0.1

The fluorescence intensity of the MNs array were strictly related to the blue shift of the PSiMB optical spectrum: as a matter of fact, the blue shift indicated a depletion of the PSiMB tank, to which corresponded a decrease of the fluorescence intensity of the MNs as the immersion time in PBS increased. We have verified that the fluorescence decrease was not due to a decay of the radiative properties of the molecules by measuring the fluorescence intensity of loaded MNs not exposed to PBS solution as a function of time, as reported in Fig. 8.

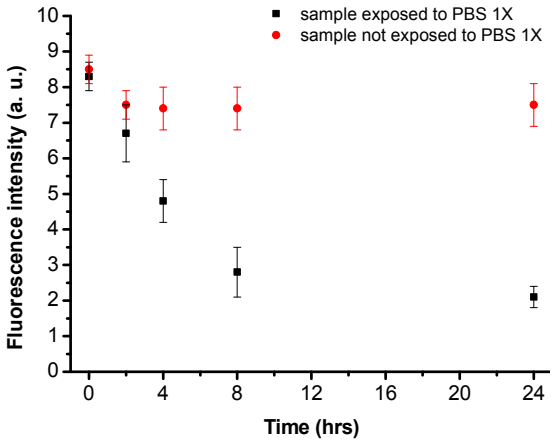

Fig. 8. Fluorescence intensity of the device changes as function of time of fluorescein release in PBS. The control shows that intensity fluorescence decreasing is not due to fluorescence decay.

After the equilibrium was reached, the fluorescent signal did not change in time, so we attributed the strong emission change of the sample exposed to PBS to a real dispersion of fluorescein in the external solution.

#253445 Received 6 Nov 2015; revised 9 Feb 2016; accepted 22 Feb 2016; published 4 Apr 2016

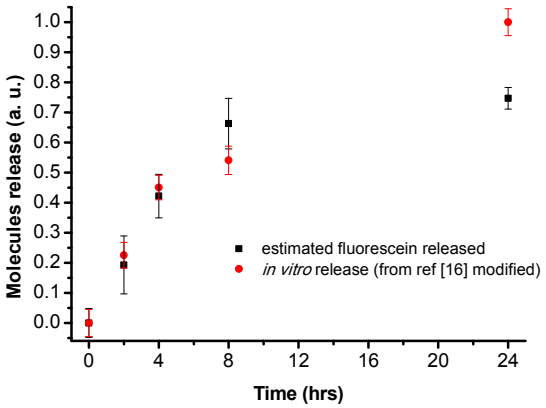

Fig. 9. Comparison between the estimated fluorescein released in PBS and data of in vitro release as reported in ref [16].

Since we attributed the decreasing of MNs fluorescence intensity to the release of fluorescein in the PBS solution, in order to confirm this hypothesis, we compared in Fig. 9 these data with those reported in [16]: methylene blue (320 Da), loaded in hydrogel-forming MNs patch, made of 15% w/w poly(methylvinylether/maelic acid) and 7.5% w/w poly(ethyleneglycol), was released and quantified in in vitro experiment [16]. If we assume that the estimated fluorescein was proportional to the complement of the fluorescence intensity, i.e. molecules released were estimated as 1-Ifn (where Ifn is the fluorescence intensity normalized to its maximum value), the comparison with respect to data reported in [16]. highlighted a really similar behavior, and the kinetic of the release was also very similar.

4. Conclusions

The hybrid patch based on polymeric MNs and PSiMB is a proof-of-concept device, which could offer several advantages in local administration of drugs since each part can be designed and tailored to match the requirements of specific application, such as total release time and rate. The porous silicon membrane guarantees a naked-eye check of drug delivery status, and, simultaneously, serves as high volume storage tank: uploading capacity scales with pore volume (porosity) of porous silicon and drug density within the pores. For melt loading, the theoretical maxima (100wt%) can be reached quite closely. For many other drugs of lower density and a silicon matrix of about 70% porosity, upon filling a 40wt% payload will result. Proteins and peptides are completely different because these scale better with accessible surface area (not necessarily total surface area): about 10-20wt% with large antibodies can be obtained [26].

Since the release of the drug molecules is due to the swelling of the polymer matrix, local dosing at very high concentration, normally prevented in case of subcutaneous injection, is easily enabled by diffusion in the physiological liquid [27].

The low-cost production techniques and the flexibility of the proposed device suggest its adoption in large area medical applications, such as vaccine administration, or long time drug delivery.

#253445 Received 6 Nov 2015; revised 9 Feb 2016; accepted 22 Feb 2016; published 4 Apr 2016